The Meteoritical Society

*Meteoritics & Planetary Science* 42, Nr 1, 3–17 (2007)
Abstract available online at http://meteoritics.org

# On the structure of mare basalt lava flows from textural analysis of the LaPaz Icefield and Northwest Africa 032 lunar meteorites

James M. D. DAY* and Lawrence A. TAYLOR

Planetary Geosciences Institute, Department of Earth and Planetary Science, University of Tennessee, Knoxville, Tennessee 37996–1410, USA
*Corresponding author. E-mail: jday13@utk.edu; dinesday@hotmail.com

*(Received 12 May 2006; revision accepted 26 October 2006)*

**Abstract–**Quantitative textural data for Northwest Africa (NWA) 032 and the LaPaz (LAP) mare basalt meteorites (LAP 02205, LAP 02224, LAP 02226, and LAP 02436) provide constraints on their crystallization and mineral growth histories. In conjunction with whole-rock and mineral chemistry, textural analysis provides powerful evidence for meteorite pairing. Petrographic observations and crystal size distribution (CSD) measurements of NWA 032 indicate a mixed population of slowly cooled phenocrysts and faster cooled matrix. LaPaz basalt crystal populations are consistent with a single phase of nucleation and growth. Spatial distribution patterns (SDP) of minerals in the meteorites highlight the importance of clumping and formation of clustered crystal frameworks in their melts, succeeded by continued nucleation and growth of crystals. This process resulted in increasingly poor sorting, during competition for growth, as the melt crystallized. Based on CSD and SDP data, we suggest a potential lava flow geometry model to explain the different crystal populations for NWA 032 and the LaPaz basalts. This model involves crystallization of early formed phenocrysts at hypabyssal depths in the lunar crust, followed by eruption and flow differentiation on the lunar surface. Lava flow differentiation would allow for formation of a cumulate base and facilitate variable cooling within the stratigraphy, explaining the varied textures and modal mineralogies of mare basalt meteorites. The model may also provide insight into the relative relationships of some Apollo mare basalt suites, shallow-level crystal fractionation processes, and the nature of mare basalt volcanism over lunar history.

## INTRODUCTION

Textures of igneous rocks result from the dynamics of crystal nucleation and growth, which in turn reflect magmatic cooling regimes (Kirkpatrick 1977, 1981, 1983; Marsh 1998). Proliferation and continued development of the crystal size distribution (CSD) quantitative textural analysis technique has greatly improved understanding of igneous crystallization processes and provides information on time scales and mineral histories of magmatic systems (Marsh 1988, 1998; Cashman and Marsh 1988; Higgins 2000, 2002). CSD analysis also has great promise as a quantitative tool for understanding the nature of planetary magmatic systems, especially where detailed field data and other structural constraints may be lacking. For example, studies of Martian nakhlites have demonstrated that these cumulative clinopyroxene-rich rocks are probably from the same or related flows on Mars, with similar stratigraphies to terrestrial ultra-mafic or komatiite flows (Day et al. 2006a; Lentz et al. 1999). In this way, quantitative textural analysis allows inferences to be made on the emplacement and nature of igneous rocks, the growth rate of crystals, crystal fractionation, and the evolution of magmatic systems.

So far, only a few CSD studies have been performed on lunar rocks, with examples available for impact-melt and metamorphic breccias (Cushing et al. 1999), and for mare basalts (Day et al. 2005). This is surprising, considering the limited information available regarding the kinetics of magma crystallization on the Moon. Aluminum-rich basalts and a KREEP basalt have also been analyzed for quantitative textural parameters (Lentz and Taylor 2002). In this study, we present new quantitative textural data for Northwest Africa (NWA) 032 and the LaPaz (LAP) mare basalt meteorites (LAP 02205, LAP 02224, LAP 02226, LAP 02436, and LAP 03632). These basalts have similar ages and geochemical compositions and have been considered as crater-source or launch paired meteorites from the same lunar magmatic system. Here, CSD and size distribution pattern (SDP) data are used to explore the kinetics of crystallization in these basalts and the implications these have for understanding experimental cooling rate estimates in mare basalts, the petrological and geochemical evolution of basaltic lava flows, and the significance of textures for meteorite pairing.

## PETROGRAPHIC AND GEOCHEMICAL BACKGROUND

Since their discovery, the LaPaz and NWA 032 mare basalts have received considerable attention because they represent two of only eight unbrecciated mare basalt meteorites discovered on Earth to date (the others are Yamato-793169, Asuka-881757, Dhofar 287, NWA 773/2700/2977, NWA 3160/2727, and NWA 003—note that the latter four meteorites have relatively small portions of basaltic breccia material attached). Furthermore, NWA 032 and the LaPaz lunar meteorites represent young (~3 Gyr), low-Ti, evolved mare basalts with elevated incompatible element abundances. These attributes make them distinct from the Apollo and Luna collections of mare basaltic material.

Northwest Africa 032 was discovered in the Sahara desert region in 1999 and has been described in detail by Fagan et al. (2002). The LaPaz basalts, which include LAP 02205, LAP 02224, LAP 02226, LAP 02436, and LAP 03632, were discovered in the LaPaz ice field in 2002–2003 and have been characterized by Anand et al. (2006), Day et al. (2006b), Joy et al. (2006), Righter et al. (2005), and Zeigler et al. (2005). We note that all studies of the LaPaz basalts presented to date consider them to be crater-source or launch paired with NWA 032. This pairing relationship extends to exposure ages, with the LaPaz basalts reputed to have been ejected from the Moon at 55 ± 5 kyr (Nishiizumi et al. 2006). Based on cosmogenic radionuclide data, the ejection age of NWA 032 is 47 ± 10 kyr (Nishiizumi and Caffee 2001), which is indistinguishable from the ejection age of the LaPaz basalts. Crystallization ages for the LaPaz basalts and NWA 032 have been obtained via numerous methods, with at least five different reported ages for LAP 02205. Ar-Ar age dating of NWA 032 yields a whole-rock age of 2.78 ± 0.01 Gyr (Fagan et al. 2002; Fernandes et al. 2003), which is outside the error of the Ar-Ar ages of 2.95 ± 0.02 Gyr (Nyquist et al. 2005), and 2.92 ± 0.01 Gyr (Fernandes and Burgess 2006), reported for LAP 02205. The younger age of NWA 032 could relate to recoil of $^{39}$Ar, or the presence of preshock $^{40}$Ar incorporated in the pervasive melt veins within the sample studied by Fernandes et al. (2003). Rb-Sr isochron studies of LAP 02205 have yielded similar initial crystallization ages of 3.02 ± 0.03 Gyr (Nyquist et al. 2005) and 2.96 ± 0.01 Gyr (Rankenburg et al. 2005). U-Pb age dating of phosphates in LAP 02205 yielded an isochron age of 2.93 ± 0.15 Gyr (Anand et al. 2006). Apparent ages for LAP 02205 are, therefore, in good agreement; the Ar-Ar age results perhaps yielding younger ages compared to the Rb-Sr and U-Pb methods for similar reasons to the complex Ar age spectra in NWA 032. Based on the cosmic exposure and crystallization ages, it appears that NWA 032 and the LaPaz basalts formed at ~2.9 Gyr and were expelled from the Moon during the same impact event at ~0.05 Myr.

The most significant differences between NWA 032 and the LaPaz mare basalt meteorites are their textures and mineral modes. NWA 032 is a porphyritic basalt with phenocrysts of olivine, pyroxene, and chromite set in a crystalline, plumose- or quench-textured groundmass of plagioclase, pyroxene, ilmenite, troilite, and FeNi metal (Fig. 1) (Fagan et al. 2002). The LaPaz basalts are holocrystalline intergranular-to-subophitic basalts that are predominantly composed of pyroxene, plagioclase, and ilmenite, with accessory phases of silica, olivine, spinel, phosphates, troilite, FeNi metal grains, and zirconium-rich minerals (Fig. 1) (Day et al. 2006b). These basalts possess a network of brown shock-melt veins, and all have similar mineral assemblages and compositions. Both meteorites have similar olivine ($Fo_{65–67}$) and plagioclase core compositions (NWA 032, $An_{80–90}$; LaPaz, $An_{79–93}$), and a near-identical range in oxides, with high-Al chromites in olivine cores, and ilmenite forming toward the end of the crystallization sequence (Anand et al. 2006; Day et al. 2006b; Righter et al. 2005; Zeigler et al. 2005). Pyroxene core compositions for the meteorites are also similar (Molar Mg/(Mg + Fe) × 100 = 50–70) (Zeigler et al. 2005). However, there are some contrasting features, especially for pyroxene rim compositions. For example, NWA 032 possesses a more restricted and slightly lower-Ca range of ferro-pyroxenes to the LaPaz basalts, and more calcic and less magnesian cores. The differences in pyroxene and also Fe-Ti oxide compositions likely relate to the more rapid crystallization of the matrix of NWA 032. Lofgren et al. (1974) argued that rapidly cooled pyroxene crystals have preferential uptake of Ca-Fe-Al-Ti relative to Mg-Si, which would result in Ca depletion in the residual liquid.

There are similarities in whole-rock compositions for the LaPaz basalts and NWA 032. Major element compositional differences for the two basalts can be explained by variable fractionation of olivine, chromite (Day et al. 2006b), and Mg pyroxene (Zeigler et al. 2005) between NWA 032 (more Mg-rich) and the more fractionated LaPaz basalts. Furthermore, these samples lie on similar fractionation trends (Day et al. 2006b; Righter et al. 2005; Zeigler et al. 2005). Perhaps most revealing are the near-identical rare earth element patterns for the meteorites, which are more incompatible-element-enriched than low-Ti Apollo 12 mare basalts and some low-Ti lunar glass beads (Day et al. 2006b). Therefore, the only real differences between the LaPaz basalts and NWA 032 are their textures and modal mineralogies. Qualitatively, the LaPaz basalts possess textures indicative of slow cooling (0.1–1 °C $hr^{-1}$) (Anand et al. 2006; Day et al. 2006b), whereas NWA 032 has a two-stage cooling history of slowly

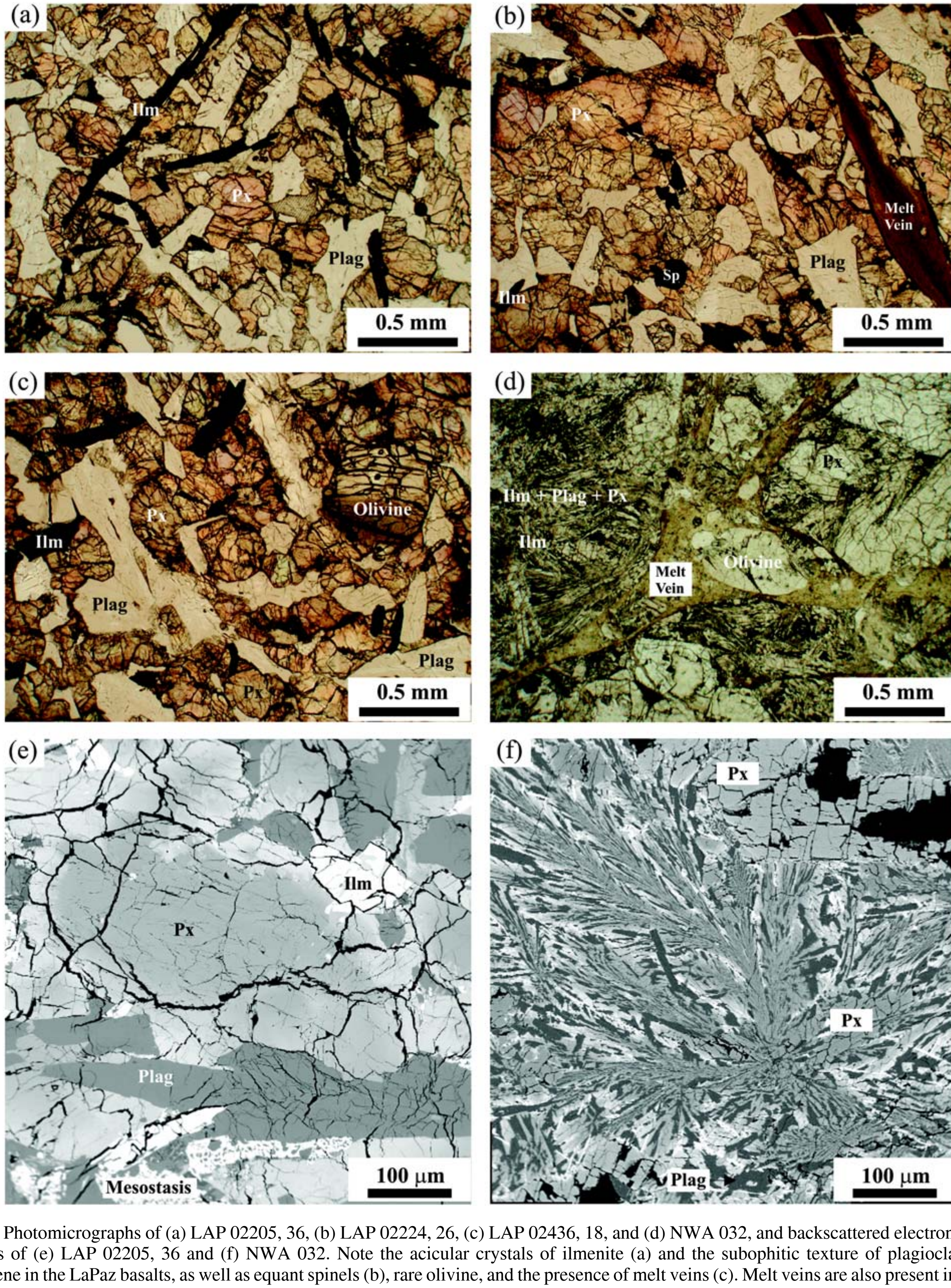


Fig. 1. Photomicrographs of (a) LAP 02205, 36, (b) LAP 02224, 26, (c) LAP 02436, 18, and (d) NWA 032, and backscattered electron (BSE) images of (e) LAP 02205, 36 and (f) NWA 032. Note the acicular crystals of ilmenite (a) and the subophitic texture of plagioclase and pyroxene in the LaPaz basalts, as well as equant spinels (b), rare olivine, and the presence of melt veins (c). Melt veins are also present in NWA 032 (d). Pyroxenes in the LaPaz basalts are strongly zoned and mesostasis areas abut the edges of the major crystal phases (e). By comparison, the texture of the matrix in NWA 032 is very different from the LaPaz basalts, with plumose-textured intergrowths of pyroxene, plagioclase, Fe-Ti oxides, and silica (f) similar to that of "clast K" in mare basalt breccia MET 01210 (Day et al. 2006c).

crystallized phenocrysts (<2 °C $hr^{-1}$) set within a fast-cooled matrix (20–60 °C $hr^{-1}$) (Fagan et al. 2002). In this study, we quantitatively analyze the textures of NWA 032 and the LaPaz basalts and seek to explain differences between these meteorites in terms of their mineral modes and crystallization histories.

## CRYSTAL SIZE DISTRIBUTION AND SPATIAL DISTRIBUTION PATTERN ANALYSIS

Crystal size distribution analysis is a well-established and statistically viable tool for quantitative petrographic analysis of igneous and metamorphic rocks (Marsh 1998; Higgins 2000). Quantification of crystal population densities of a phase at a given size interval can be used, via a CSD plot, to gain information regarding crystal growth histories. CSD theory is based on the concept that the crystallizing system achieves steady-state conditions, whereby continuous nucleation and growth produce a skewed distribution of grain sizes, thus generating a negative linear plot in population density-crystal size space. The population density ($n$) of the articles in question (crystals, vesicles, etc.) is linked to their size ($L$); whereas growth rates ($G$), residence time ($\tau$), and final nucleation density ($n_0$) are constant for an individual CSD such that:

$$n = n_0 \exp(-L/G\tau) \quad (1)$$

This theoretical relationship is only valid in a steady-state open system. CSDs are often not straight lines, but individual straight portions of the CSD plot may be regressed. Linear regression analysis of the CSD curve provides a measure of growth rate/residence time (slope) and nucleation density (intercept). In addition, the shape of the CSD curve can reveal the operation of different processes during crystallization of magma batches (Marsh 1998). Spatial distribution pattern (SDP) analysis is a quantitative means of assessing the arrangement of spatially related crystal constituents with R values (SDP) (Jerram et al. 1996). SDP distinguishes touching crystal frameworks and provides a method to quantify the packing arrangement of crystals in the rock. The R value can be used to determine the clustering of touching crystal frameworks by comparison with the distribution of randomly packed spheres (Jerram et al. 1996, 2003). The R value is defined as:

$$\mathrm{R} = (2\sqrt{\rho}\Sigma r)/N \quad (2)$$

where $\rho$ is the density of the observed distribution, $r$ is the nearest neighbor (center-to-center) distance, and $N$ is the total number of individuals measured.

For quantitative CSD analysis, crystal measurements were performed on digital photomicrographs of polished thin sections of LAP 02205, LAP 02224, LAP 02226, and LAP 02436, to determine porosity (percentage melt), XY grain center coordinates, orientations, and lengths (long and short axis), following the protocols of Jerram et al. (2003). This technique involves the identification and outlining of crystals and conversion of the monomineralic texture to a digital bitmap image, after which each crystal is identified individually using a polarizing microscope prior to processing, using image-analysis software (Image Tool) (Fig. 2). Individual crystals were traced by hand onto an overlay. Tracing crystals by hand reduces bias toward larger crystal sizes by allowing touching crystals and glomerocrysts to be identified and separated. Because of the lack of available thin sections for NWA 032, we performed tracings of phenocrystic pyroxene and olivine crystals from an X-ray image from Fagan et al. (2002) (Fig. 1); use of these lower-resolution images results in a larger uncertainty for the results as optical identification and separation of touching crystals was not possible. Resulting quantitative textural information is used to provide CSD and spatial distribution patterns. Digitized images were processed using freeware (Image Tool), and 3-D crystal dimensions were predicted using the method of Morgan and Jerram (2006). Stereological corrections for 3-D CSD patterns were made using CSD correction software (CSD corrections, version 1.36) (Higgins 2000). R-values were calculated according to the technique of Jerram et al. (1996) using Big-R software (M. J. Higgins, unpublished).

## RESULTS

### CSD and SDP Analysis

Crystal size distribution data and R values for ilmenite, plagioclase, pyroxene, and olivine in the LaPaz and NWA 032 basalts are presented in Table 1 and Fig. 3. The representative grain aspect ratios, based on 3-D crystal dimension predictions (Morgan and Jerram 2006) and employed for CSD correction were 1.0:2.0:5.3, 1.0:1.5:1.5, 1.0:1.5:1.5, and 1.0:6.0:6.0 for plagioclase, pyroxene, olivine, and ilmenite, respectively. Textural analysis for pyroxene was only performed for two samples and yielded broadly similar average length and width data, with NWA 032 pyroxenes (0.32 × 0.11 mm) being slightly more elongate than those of LAP 02205 (0.28 × 0.17 mm). Analysis of the olivine fraction in NWA 032 was restricted to 134 grains (normally in excess of 250 grains are required for statistically valid 3-D CSD corrections) (Morgan and Jerram 2006), leading to greater uncertainty in the interpretation of textural data. Nevertheless, a robust observation is that NWA 032 olivines have larger average grain sizes than pyroxenes in the same sample (0.45 × 0.24 mm). By comparison, olivines in the LaPaz basalts are estimated as having average lengths between 0.1 and 0.3 mm (Zeigler et al. 2005). Pyroxene, plagioclase (0.27 × 0.10 mm), and ilmenite (0.20 × 0.06 mm) fractions all possess nearly straight CSDs for the LaPaz basalts, indicating single phase populations (Fig. 3). The log-linear relationship, which differs

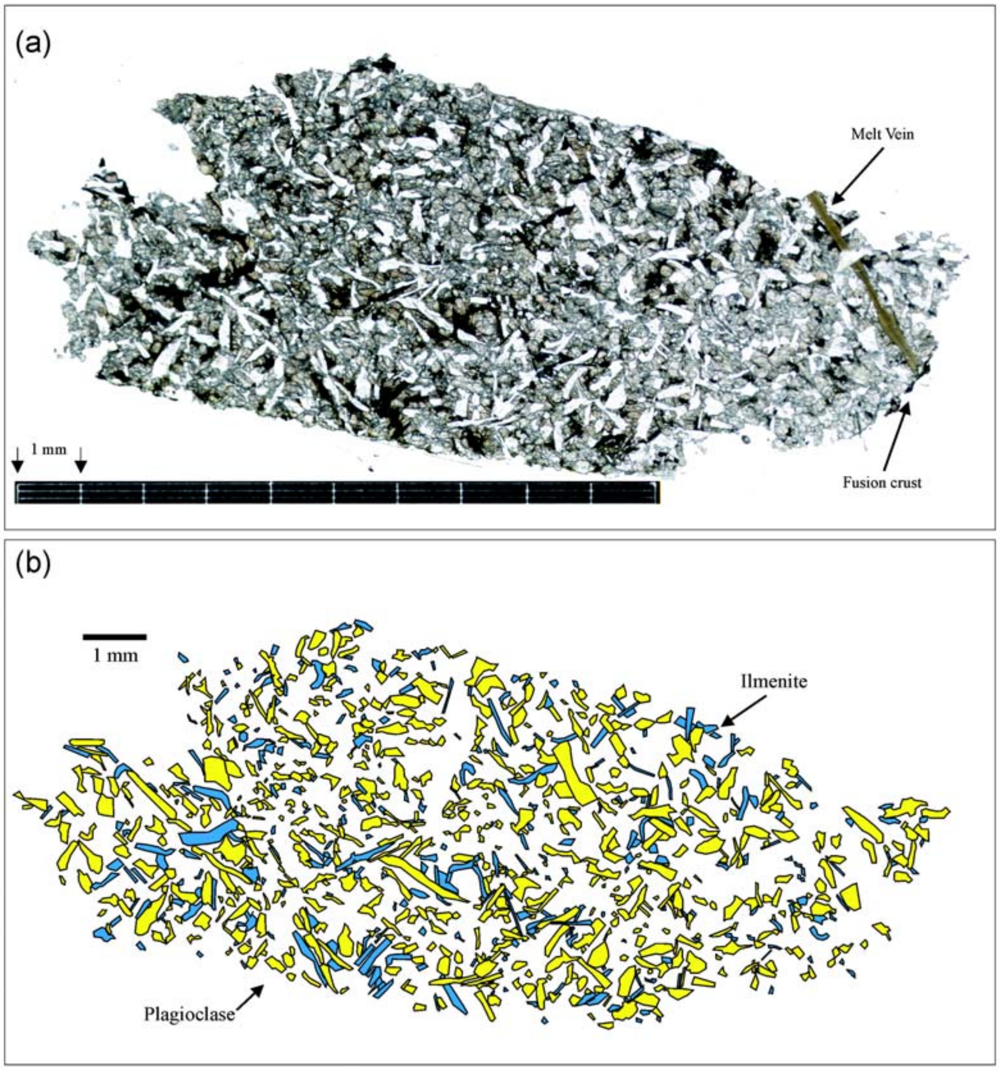


Fig. 2. A photomicrograph of (a) LAP 02224, 26 and (b) a corresponding composite digital image of traced plagioclases and ilmenites within the section. Outlines of crystals in all samples were made in this manner in order to generate quantitative textural data. The scale bar micrometer ruler in (a) is equal to 10 mm.

only slightly in pattern morphology and population density, implies that steady-state nucleation and growth were important processes in the formation of the pyroxene, plagioclase, and ilmenite populations in the LaPaz and NWA 032 mare basalts. The olivine in NWA 032 has a convex slope on a CSD plot (Fig. 3a), which may be indicative of two populations with different growth histories.

Width and length data generate broadly consistent slopes in population density versus crystal-size space for different phases, resulting in a restricted range of slopes and intercepts for olivine (length data slope = –4.4, intercept = 3.5), pyroxene (LaPaz avg. slope = –8.8 ± 0.5, avg. intercept = 7.3 ± 0.4; NWA 032 length. slope = –6.7, length intercept = 5.3), plagioclase (avg. slope = –6.6 ± 0.9, av. intercept = 6.6 ± 0.6) and ilmenite (avg. slope = –8.7 ± 1.8, av. intercept = 6.8 ± 0.7). Width data generate slightly steeper slopes for plagioclase and shallower slopes for ilmenite (Fig. 3). Slight downturns for smaller size-fractions are consistent with either shock-induced annealing (an "Ostwald ripening"–type effect where large crystals grow at the expense of smaller crystals), or cessation of nucleation accompanied by continued growth. There may also be a measurement artefact in the data because of the difficulty in obtaining accurate results for the smaller crystal-size classes due to image pixilation. Similarly, CSDs tend to diverge at larger crystal sizes due to the lower number of crystals measured and larger uncertainties in their population densities (Higgins 2002). Despite these caveats, the restricted range in average slope and average intercept values for the LaPaz mare basalts confirms "textural pairing" and provides a useful approximation of the average error associated for our analysis technique.

Table 1. Crystal size distribution and spatial distribution pattern data for the LaPaz mare basalt meteorites.

| Sample | Phase | Measurement | Area ($mm^2$) | No. of grains | Percent area | ±1SD | Average dimensions | ±1SD | Slope ($mm^{-1}$) | Intercept | R value | Shape |
|---|---|---|---|---|---|---|---|---|---|---|---|---|
| LAP 02-205, 36 | Pyroxene | Length | 52.6 | 563 | 58 | 7 | 0.28 | 0.13 | −8.46 | 7.03 | 1.35 | 1:1.2:1.8 |
| | | Width | | | | | 0.17 | 0.08 | −9.15 | 7.55 | | |
| | Plagioclase | Length | 51.6 | 542 | 40 | 7 | 0.27 | 0.16 | −6.70 | 6.45 | 1.28 | 1:1.6:5.0 |
| | | Width | | | | | 0.10 | 0.05 | −7.23 | 7.55 | | |
| | Ilmenite | Length | 44.6 | 253 | 6 | 2 | 0.21 | 0.17 | −8.68 | 6.11 | 1.09 | 1:2.9:10.0 |
| | | Width | | | | | 0.05 | 0.03 | −6.74 | 7.41 | | |
| LAP 02-224, 26 | Plagioclase | Length | 61.4 | 563 | 36 | 6 | 0.25 | 0.17 | −6.44 | 6.19 | 1.18 | 1:1.8:6.0 |
| | | Width | | | | | 0.10 | 0.06 | −6.94 | 7.25 | | |
| | Ilmenite | Length | 66.1 | 563 | 6 | 2 | 0.23 | 0.17 | −8.62 | 5.98 | 1.11 | 1:2.8:10.0 |
| | | Width | | | | | 0.07 | 0.04 | – | – | | |
| LAP 02-226, 19 | Plagioclase | Length | 76.9 | 868 | 36 | 6 | 0.24 | 0.16 | −6.98 | 6.50 | 1.17 | 1:2.0:8.0 |
| | | Width | | | | | 0.09 | 0.05 | −7.90 | 7.63 | | |
| | Ilmenite | Length | 72.9 | 369 | 4 | 1 | 0.20 | 0.15 | −9.95 | 6.35 | 1.11 | 1:2.8:10.0 |
| | | Width | | | | | 0.05 | 0.03 | – | – | | |
| LAP 02-436, 18 | Plagioclase | Length | 51.3 | 343 | 39 | 7 | 0.33 | 0.22 | −4.92 | 5.23 | 1.17 | 1:2.0:8.0 |
| | | Width | | | | | 0.12 | 0.10 | −5.56 | 6.36 | | |
| | Ilmenite | Length | 49.0 | 389 | 5 | 1 | 0.16 | 0.13 | −11.50 | 7.05 | 1.06 | 1:1.9:10.0 |
| | | Width | | | | | 0.05 | 0.03 | −6.79 | 7.71 | | |
| NWA 032 | Pyroxene[a] | Length | 89.5 | 302 | 12 | 5 | 0.32 | 0.17 | −6.68 | 5.27 | 1.12 | 1:2.3:10.0 |
| | | Width | | | | | 0.11 | 0.08 | −12.7 | 6.84 | | |
| | Olivine[a] | Length | 93.2 | 134 | 15 | 6 | 0.45 | 0.30 | −4.40 | 3.49 | 1.18 | 1:1.4:2.3 |
| | | Width | | | | | 0.24 | 0.15 | −6.00 | 4.61 | | |

[a]Only phenocryst populations analyzed by CSD.

Crystal dimensions set at: plagioclase = 1:2.5:3, pyroxene and olivine = 1:1.5:1.5, ilmenite = 1:6:6, using a calculated roundness value of 0.5.

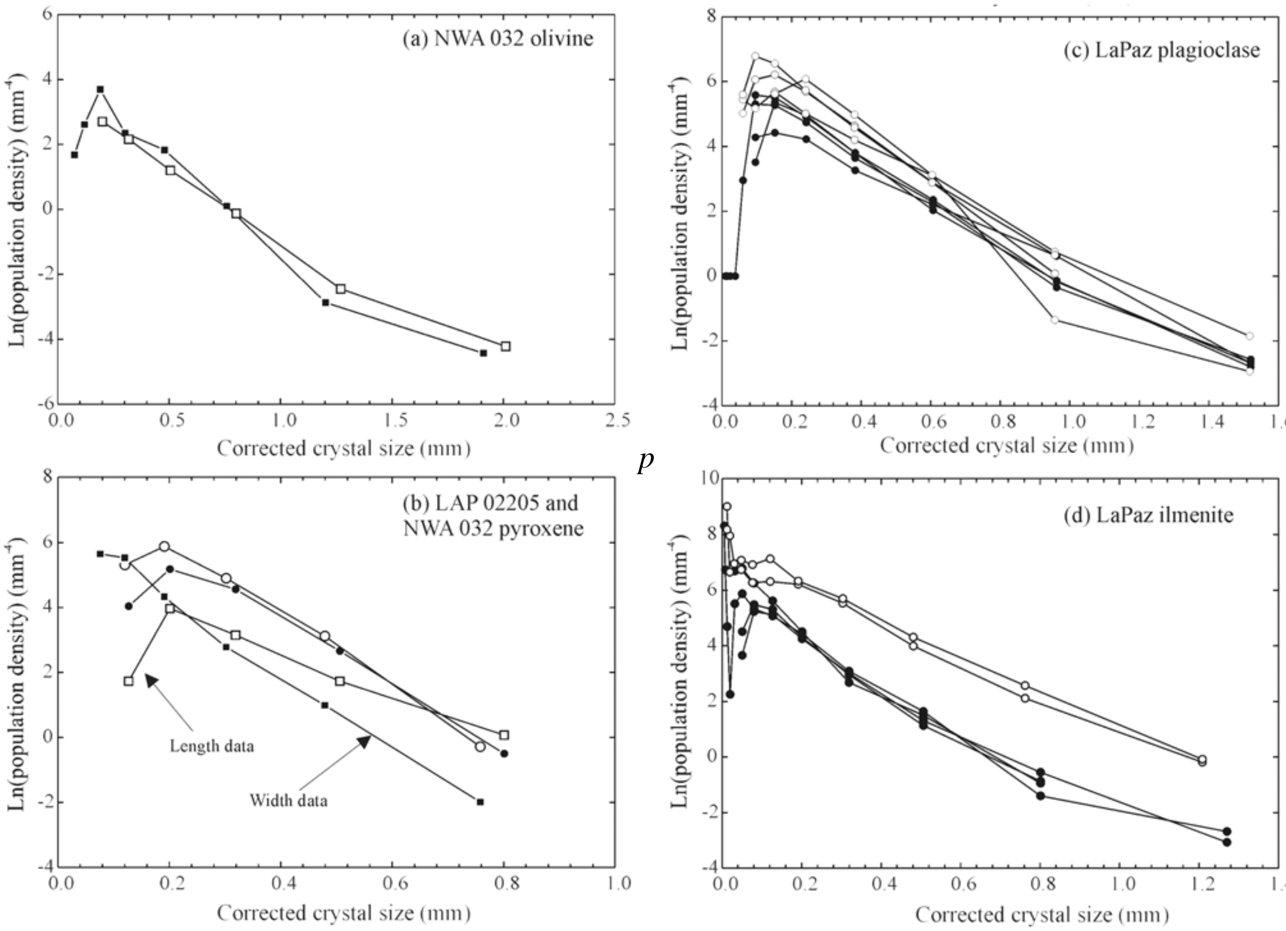


Fig. 3. Crystal size distribution (plotted as a function of corrected crystal size versus population density) diagrams for (a) NWA 032 olivine phenocrysts, (b) LAP 02205 (circles) and NWA 032 (squares) pyroxenes, (c) LaPaz plagioclase, and (d) ilmenite. Filled symbols represent data calculated from width data; unfilled symbols represent data calculated from length data. The width and length data generally compare well although the slopes and absolute population densities vary proportionally to one another.

Further evidence for the precision and validity of the CSD technique comes from comparison of modal data derived from CSD and from feature scan phase distribution (FSPD), using the method of Taylor et al. (1996). Higgins (2002) showed that there was good agreement with calculated volumetric phase proportions for plagioclases via CSD and phase proportion determinations in thin section for Mount Taranaki lavas, and suggested that agreement between these measurements indicated accurate CSD data. Comparison of modal data for NWA 032 and the LaPaz basalts (Day et al. 2006b; Fagan et al. 2002) with modal percentages derived from CSD (Table 2) show that they are in excellent agreement.

Spatial distribution pattern analyses of NWA 032 and the LaPaz mare basalts are graphically represented in Fig. 4. Porosity, as a percentage of the melt value at the time of crystallization (and henceforth termed the residual melt fraction or melt porosity) varies according to relative position in the crystallization sequence such that olivine > pyroxene ≥ plagioclase > ilmenite. Early crystallized pyroxenes and olivines (as shown from NWA 032) lie close to the random sphere distribution line, whereas the overall pyroxene population in LaPaz possesses the highest R values for a given residual melt fraction at ~50% (touching crystal framework). Ilmenites have lower R values and lower melt porosity than plagioclase as a result of their later crystallization. Both plagioclase and ilmenite are inferred to have formed at low melt porosities because they crystallize interstitial to early formed crystals and therefore were in competition for space during mineral growth. With crystallization, NWA 032 and the LaPaz basalts go from relatively ordered to increasingly clustered, touching, and poorly sorted crystal frameworks. The clustering of crystals recognized for minerals in NWA 032 and the LaPaz basalts is a common, if not ubiquitous, feature in phenocryst populations, and may represent the building blocks of all igneous rocks (e.g., Jerram et al. 2003). The statistical clustering of later crystallizing grains suggests they did not

Table 2. Comparison of FSDP and CSD modal analysis of LaPaz mare basalt meteorites and comparison with NWA 032.

| | LAP 02205,31 | | | LAP 02224,26 | | | LAP 02226,19 | | | LAP 02436,1 | | | NWA 032[a] | | | NWA 032[b] |
|---|---|---|---|---|---|---|---|---|---|---|---|---|---|---|---|---|
| Method volume% | FSPD[c] | CSD | 2σ | FSPD[c] | CSD | 2σ | FSPD[c] | CSD | 2σ | FSPD[c] | CSD | 2σ | FSDP | CSD | 2σ | |
| Pyroxene (Total) | 55.5 | 58.0 | 7.1 | 55.7 | – | – | 55.8 | – | – | 54.6 | – | – | 52.0 | – | – | 50.7 |
| (Phenocrysts) | – | – | – | – | – | – | – | – | – | – | – | – | – | 11.9 | 4.6 | 9.6 |
| Plagioclase | 33.7 | 39.7 | 7.0 | 32.2 | 35.7 | 6.2 | 32.1 | 35.9 | 5.5 | 32.8 | 39.2 | 7.3 | 29.3 | – | – | 29.4 |
| Ilmenite | 3.3 | 6.1 | 1.9 | 3.0 | 5.7 | 1.5 | 3.5 | 4.4 | 0.9 | 3.3 | 5.0 | 1.1 | 2.6 | – | – | 4.4 |
| Melt (vein, fusion) | 1.5 | – | – | 2.1 | – | – | 1.9 | – | – | 2.1 | – | – | 7.3 | – | – | 3.2 |
| Fayalite | 1.4 | – | – | 1.5 | – | – | 1.6 | – | – | 2.0 | – | – | – | – | – | – |
| Olivine | 1.2 | – | – | 1.9 | – | – | 1.3 | – | – | 1.6 | – | – | 8.1 | 15 | 6 | 11.3 |
| K-glass | 0.7 | – | – | 0.7 | – | – | 0.6 | – | – | 0.8 | – | – | 0.3 | – | – | <0.1 |
| Troilite | 0.2 | – | – | 0.2 | – | – | 0.2 | – | – | 0.2 | – | – | 0.2 | – | – | 0.7 |
| Ulvöspinel | 0.4 | – | – | 0.5 | – | – | 0.4 | – | – | 0.4 | – | – | tr. | – | – | – |
| Chromite | 0.1 | – | – | 0.2 | – | – | 0.1 | – | – | 0.1 | – | – | 0.3 | – | – | 0.3 |
| Phosphate | 0.3 | – | – | 0.2 | – | – | 0.2 | – | – | 0.2 | – | – | tr. | – | – | – |
| FeNi metal | tr. | – | – | tr. | – | – | tr. | – | – | tr. | – | – | tr. | – | – | tr. |

[a]Modal analysis data by feature scan phase distribution (FSPD) using energy dispersive spectrometer measurements; data bins and parameters are similar to those for the LaPaz mare basalt modes (Day et al. 2006b).

[b]Data from Fagan et al. (2002).

[c]FSPD measurements from Day et al. (2006b).

tr. = trace.

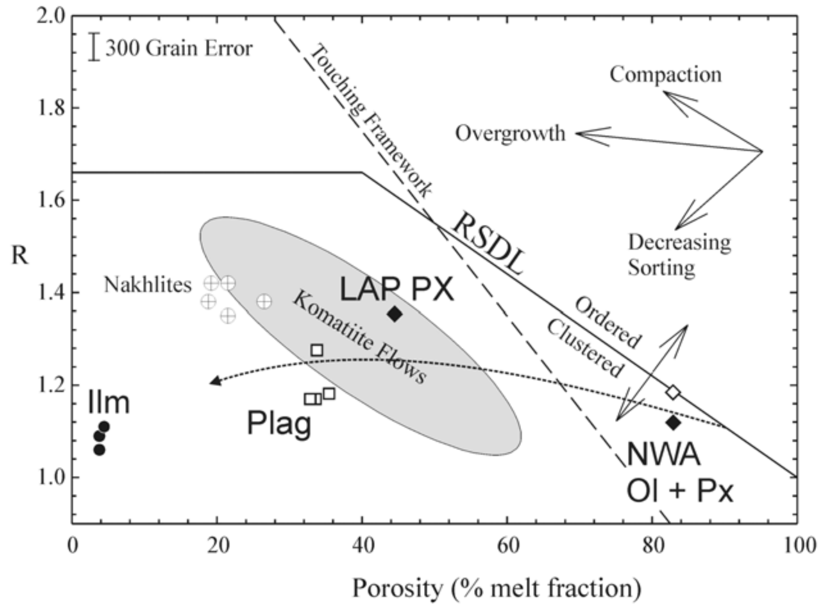


Fig. 4. A cluster analysis diagram (after Jerram et al. 2003) for NWA 032 phenocrysts and LaPaz pyroxene, plagioclase, and ilmenite crystals. Also shown are Martian nakhlites (Day et al. 2006a; Lentz et al. 1999) and the field of data for olivine from komatiitic flows. With decreasing melt porosity, the degree of sorting decreases and clustering increases in LaPaz minerals; this has important implications for the nature of crystallization for mare basalts and suggests that clustered crystal frameworks are significant during lava flow emplacement on the Moon. The dashed line indicates the relative order of crystallization of the respective minerals. RSDL = random sphere distribution line; it represents the SDP of randomly packed spheres of differing modal abundance (see Fig. 3 of Jerram et al. 2003).

form and accumulate as individuals, but rather formed via poor sorting during accumulation as clumps. In this respect, NWA 032 and the LaPaz basalts are similar to most terrestrial komatiitic and basaltic lava flows (e.g., Jerram et al. 2003) and Martian nakhlites (Day et al. 2006a; Lentz et al. 1999) analyzed with the SDP technique.

## Calculated Cooling Rates and Growth Rates

The linear plots of population density versus crystal size for NWA 032 and the LaPaz basalts in Fig. 3 have slopes that are equal to $-1/(G\tau)$ (Marsh 1998). This relationship means that crystallization rates (or cooling rates and residence times) for crystals can be calculated if a growth rate is estimated. In order to calculate cooling rates and residence times, we have employed independently calculated cooling rates from plagioclase lath thickness (Anand et al. 2006; Day et al. 2006b) to estimate growth rates for NWA 032 olivine and pyroxene and LaPaz pyroxenes, plagioclase, and ilmenite. These growth rates have been calculated to be ~$3 \times 10^{-8}$ mm/s (Table 3), consistent with, if not faster than, estimates of minerals in terrestrial basalt lava flows (e.g., Cashman and Marsh 1988; Marsh 1998; Jerram et al. 2003). It should be noted that if faster growth rates are used, cooling rates will increase and estimated crystallization time will decrease. Cooling rates for LaPaz pyroxene, plagioclase, and ilmenite can be calculated at 0.21 ± 0.01 °C $hr^{-1}$, 0.15 ± 0.02 °C $hr^{-1}$ and 0.20 ± 0.04 °C $hr^{-1}$, respectively, over a crystallization temperature range of ~200 °C (the estimated range from MELTS program models) (Anand et al. 2006) using these growth rates. These are similar to independent cooling rate calculations for the LaPaz basalts (0.1–1 °C $hr^{-1}$) (Anand et al. 2006; Day et al. 2006b) using the methods of Grove and Walker (1977) and Lofgren et al. (1974). Cooling rates for NWA 032 olivine and pyroxene are calculated as 0.12 ± 0.02 °C $hr^{-1}$ and 0.23 ± 0.07 °C $hr^{-1}$, respectively, over the same ~200 °C crystallization range. These are somewhat lower than the estimated growth rate for phenocrystic olivine by Fagan et al. (2002) of <2 °C $hr^{-1}$ based on morphological comparisons with experimentally grown olivine (Donaldson 1976). Based on the consistency of cooling rates in LaPaz silicate minerals (~0.2 °C $hr^{-1}$) with that of ilmenite (0.2 °C $hr^{-1}$) in the LaPaz basalts, there is no reason to assume that oxide growth rates should differ from those of silicate minerals. For example, if the calculated terrestrial ilmenite growth rate of Cashman and Marsh (1988) of 0.34 to $0.49 \times 10^{-9}$ mm/s is applied to LaPaz ilmenites, a cooling rate equal to 1.28 ± 0.27 °C $hr^{-1}$ is derived.

Employing estimated cooling rates (~0.2 °C $hr^{-1}$), an initial eruption temperature of 1180–1220°C (Fagan et al. 2002; Day et al. 2006b), and an estimated crystallization temperature range of ~200 °C (Anand et al. 2006) for olivine, pyroxene, plagioclase, and ilmenite, we calculate that the LaPaz basalts and NWA 032 crystallized over a period in excess of 40 days, with the phenocryst olivine population for NWA 032 crystallizing over greater than twice this time period.

Table 3. Growth rates and residence time estimates for the LaPaz mare basalts.

| Sample | Phase | Measurement | Cooling rate (°C/hr) | Growth rates $\times 10^{-8}$ mm/s |
|---|---|---|---|---|
| LAP 02-205, 36 | Pyroxene | Length | 0.20 | 2.74 |
| | | Width | 0.21 | 2.53 |
| | Plagioclase | Length | 0.16 | 3.54 |
| | | Width | 0.17 | 3.20 |
| | Ilmenite | Length | 0.20 | 2.67 |
| | | Width | 0.16 | 3.43 |
| LAP 02-224, 26 | Plagioclase | Length | 0.15 | 3.59 |
| | | Width | 0.16 | 3.34 |
| | Ilmenite | Length | 0.20 | 2.69 |
| | | Width | – | – |
| LAP 02-226, 19 | Plagioclase | Length | 0.16 | 3.32 |
| | | Width | 0.18 | 2.93 |
| | Ilmenite | Length | 0.23 | 2.33 |
| | | Width | – | – |
| LAP 02-436, 18 | Plagioclase | Length | 0.11 | 4.70 |
| | | Width | 0.13 | 4.16 |
| | Ilmenite | Length | 0.27 | 2.01 |
| | | Width | 0.16 | 3.41 |
| NWA 032 | Pyroxene | Length | 0.16 | 3.47 |
| | | Width | 0.30 | 1.82 |
| | Olivine | Length | 0.10 | 5.26 |
| | | Width | 0.14 | 3.86 |

Cooling rate estimated using a growth rate from Cashman and Marsh (1988) equal to $5.4 \times 10^{-10}$ cm/s$^{-1}$. Growth rate for phases calculated from independent cooling rate estimates from the LaPaz mare basalts of 0.1–1°C/hr. Shown are growth rates for 1°C/hr.

### Growth Rates and Mineral Chemistry

In addressing the origin and nature of textural features in NWA 032 and the LaPaz mare basalt meteorites, it is useful to compare textures with mineral compositions. Mineral compositions are a direct function of the melt from which they crystallize. There is also an apparent relationship between melt composition and crystallization rates (e.g., Lofgren et al. 1974). Pyroxene and olivine in NWA 032 and the LaPaz basalts show chemical zonation (Fig. 5), which is consistent with closed-system crystallization. The most significant crystal-chemical variation occurs at the downturn for smaller size fractions in a CSD plot (Fig. 5). This relationship indicates that the Fe-rich rims of pyroxenes and olivines correspond to late-stage overgrowth on pre-existing crystals, and lack of nucleation and growth of small crystals—a variant of the Ostwald ripening effect.

It is notable that zoning in the pyroxene and large (phenocrystic/xenocrystic) olivine in NWA 032 and the LaPaz basalts is inconsistent, and where NWA 032 phenocrysts touch, they can show a lack of zonation (see Figs. 4 and 5 of Fagan et al. 2002). Where LaPaz pyroxenes and olivine abut later-formed minerals or mesostasis, they generally exhibit Fe-Mg zonation (Fig. 5). Lack of zonation in abutting phenocrysts, such as those in NWA 032, have previously been interpreted to reflect the clumping of early formed crystals in magmas (Jerram et al. 2003; Day et al. 2006a) and can be used to constrain the relative timing of clumping as prior to the crystallization of later phases (e.g., plagioclase and ilmenite) for NWA 032. The olivine and pyroxene populations in NWA 032, therefore, were clumped prior to crystallization of the finer-grained matrix, in contrast to LaPaz pyroxene and olivine, which witnessed continued growth during crystallization (Fig. 5). Assuming NWA 032 and the LaPaz basalts are related to the same magmatic system (e.g., a lava flow or sill), the time frame of mineral growth in NWA 032 and the LaPaz basalts suggests that olivine, chromite, and Mg-pyroxene fractionation, required to explain the differences in bulk compositions between the two basalts, occurred subsequent to lava flow or sill emplacement and prior to the late stages of crystallization in these basalts.

## DISCUSSION

NWA 032 and the LaPaz mare basalts have very different textures, yet the calculated cooling rates for phenocryst phases (pyroxene and olivine) in NWA 032 are very similar to those of ilmenite, pyroxene, and plagioclase in the LaPaz basalts (~0.2 °C hr$^{-1}$). It is apparent that NWA 032 and the LaPaz basalts are compositionally paired. CSD data supports source-crater or launch pairing, with obvious differences evident for the cooling histories, accumulation, and

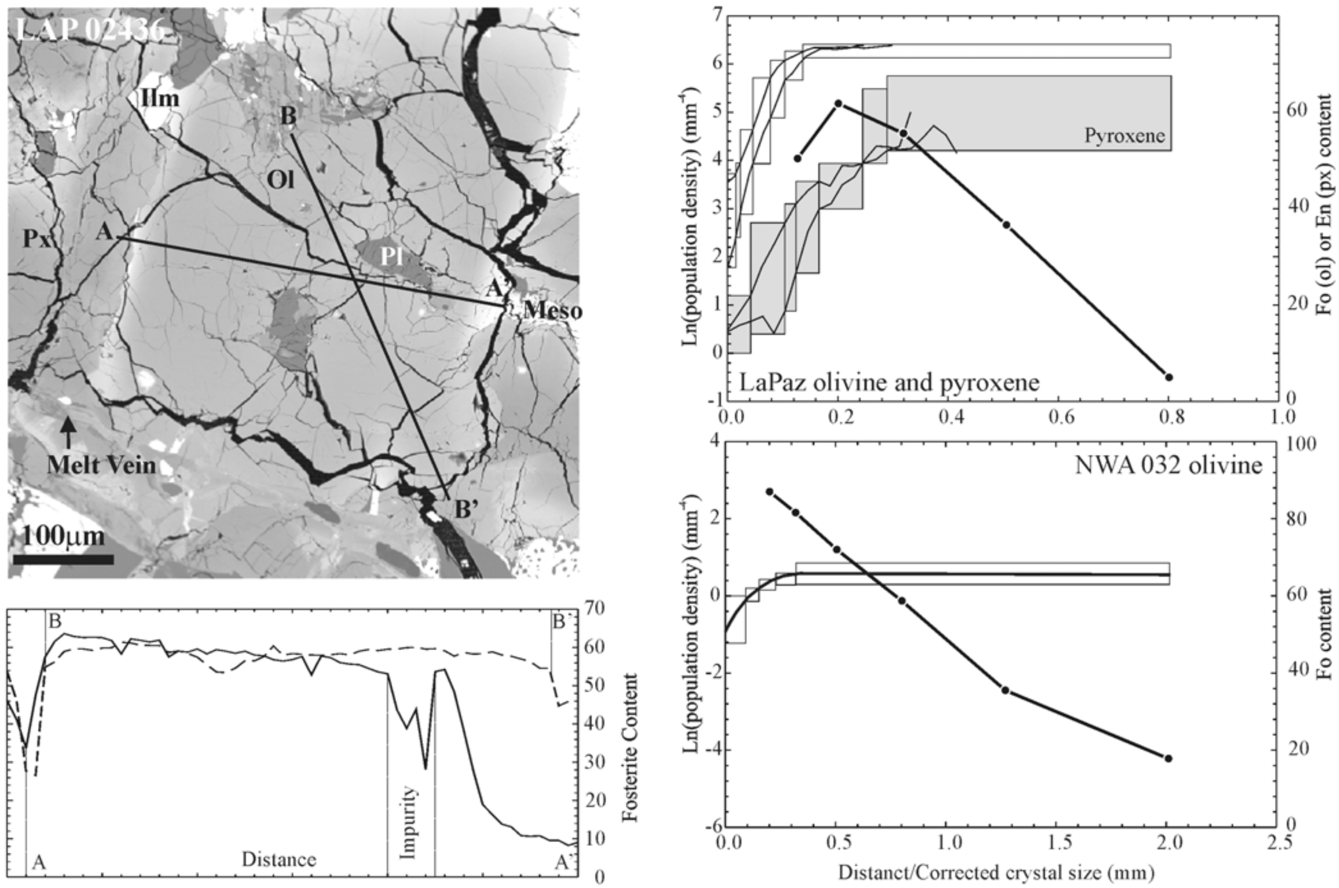


Fig. 5. A BSE image of an olivine in LAP 02436 with corresponding forsterite content profiles (A-A' and B-B') measured by electron microprobe (see Day et al. 2006b for analytical details). Note the extreme primary igneous zonation at the rims of the olivine. Also shown are composite corrected size versus population density and distance (corrected to true size) versus forsterite or enstatite contents for olivine and pyroxene in NWA 032 (lower diagram) and LaPaz mare basalts. The zonation in phenocryst minerals in NWA 032 and in pyroxenes and olivines in the LaPaz basalts occurs at the downturn in small size fractions, indicating that these downturns may relate to lower nucleation rates in the melt.

fractionation of minerals. In the following discussion, the quantitative textural measurements of these meteorites are considered in the context of experimentally derived lunar crystal growth rates and chemistry to explore the information CSD may provide regarding the thickness and stratigraphy of mare basalt lava flows.

Experimental studies provide an invaluable perspective on textural development by linking measured textures to controlled thermal conditions. Much work on reproducing natural system magma kinetics experimentally (1-Atm.) has focused around mare basalt crystallization (e.g., Lofgren et al. 1974; Usselman et al. 1975; Donaldson et al. 1975; Nabelek et al. 1978; Onarato et al. 1978). These studies have shown that when the time scale of cooling is short relative to the kinetic time scale, crystallization is highly ineffective (Lofgren 1980; Kirkpatrick 1981; Marsh 1998). Additionally, experiments of natural systems have tended to concentrate on nucleation, growth rates, and crystal morphologies as a function of undercooling, due to the technical difficulties and practical limitations (sample size and duration) of performing these experiments (e.g., Lofgren 1980; Lofgren et al. 1974; Usselman et al. 1975; Donaldson et al. 1975; Donaldson 1976, 1979; Nabelek et al. 1978). Based on these studies, the phenocryst population of NWA 032 and the ilmenite, plagioclase, and pyroxene populations of LAP 02205/02224/02226/02436 are assumed to have formed at cooling rates of <2.7 to <1.2 °C $hr^{-1}$ (Lofgren et al. 1974; Donaldson et al. 1975). Conversely, the plumose-textured matrix of NWA 032 appears to have formed in the range of 20–60 °C $hr^{-1}$ (Fagan et al. 2002).

CSD and plagioclase lath thickness (Grove and Walker 1977) growth rates can differ by an order of magnitude from the cooling rates estimated by experimental methods. Nevertheless, experimental studies have consistently provided first-order approximations of the textures seen in natural magmatic systems. Using experimental cooling rates equal to 1–2 °C $hr^{-1}$ yield much shorter residence (crystallization) times than estimated here (2–4 days versus 40 days), which would translate to faster growth rates. Cashman and Marsh (1988) used well-constrained Hawai'ian lava lake samples to obtain growth rates for plagioclase, ilmenite, and magnetite. The growth rates derived from that work are significantly slower than growth rates estimated here for NWA 032 and the LaPaz basalt crystals. This discrepancy may relate to observations that growth rates vary inversely with cooling rate (Cashman 1993), which in turn relates to the melt thickness of the lava lake studied (~80 m) (Cashman and Marsh 1988). Grove and Walker (1977) suggested a relationship between cooling rate and flow thickness for mare basalt lava flows, where estimated cooling rates equal to 0.2–0.8 °C $hr^{-1}$ correspond to a lava flow thickness of ~10–20 m.

It has been previously noted that the order of magnitude differences in growth rates between the phenocryst population and matrix in NWA 032 require formation of the phenocrysts at hypabyssal levels prior to rapid cooling of the matrix upon eruption (Fagan et al. 2002). Similar eruption dynamics have been postulated for Apollo 12 olivine basalt magmas (Donaldson et al. 1975). Based on these arguments, we suggest a simple scenario for the formation of a postulated parental lava flow (or shallow level dyke or sill) for NWA 032 and the LaPaz basalts. After melt extraction from the mantle source, solidus temperatures for olivine, chromite, and Mg-pyroxene were reached and these minerals crystallized in dykes or magma chambers in the lunar crust. Using the olivine and pyroxene growth rates in NWA 032, we estimate this to have occurred over a period of ~40–80 days. A crystal-laden (olivine, chromite, and Mg-pyroxene) magma was subsequently erupted to the lunar surface where the low melt viscosity (≤3 Pascal seconds) (Fagan et al. 2002) facilitated accumulation at the base of the flow leaving the middle of the flow relatively free of accumulated crystals (Fig. 6). In this scenario, the LaPaz basalts can be related to NWA 032. The LaPaz basalts come from the more slowly cooled middle portion of the flow, whereas NWA 032 originates from the faster-cooled flow top or base. Variable cooling rates indicate the center of the flow crystallized over a period of ~40 days, whereas the chilled margins of the flow cooled significantly faster (based on NWA 032, <10 hr). The model proposed here is similar to those of terrestrial basaltic and komatiitic magmas and to the Martian nakhlites, but also emphasizes the difference in melt viscosity for mare basalts compared with terrestrial and Martian magmas, which in turn governs crystal settling. The exceptionally low calculated melt viscosities of mare basalt magmas (close to the viscosity of water) will facilitate crystal accumulation in lava flows and magma-holding chambers and may explain the relatively low MgO content and lack of entrained xenolithic materials in mare basalt hand specimens.

This model may also be used to explain the textures and mineralogies of other mare basalts, including lunar mare basalt meteorites. For example, some recently discovered lunar meteorites have similar geochemical compositions and ages to NWA 032 and the LaPaz basalts; their mineralogies and textures seem to conform to the lunar lava flow model presented here. NWA 773 is an olivine gabbro cumulate rock with an attached breccia lithology (Jolliff et al. 2003) and has been considered compositionally paired with NWA 2700/2727 and 2977 (Bunch et al. 2006). It has a young age, elevated incompatible element geochemical signature, and a cosmic-ray exposure age similar to the NWA 032 and LaPaz basalts (Fagan et al. 2003; Fernandes et al. 2003; Jolliff et al. 2003; Borg et al. 2004; Fernandes and Burgess 2006). Olivine core (~$Fo_{68}$) and plagioclase (~$An_{90}$) compositions are also like those found in NWA 032 and the LaPaz basalts, and major (cumulate) mineral components of NWA 773 are chromite, olivine (~50 vol%), and pigeonite (Fagan et al. 2003; Jolliff et al. 2003), minerals implicated in the compositional variations between NWA 032 and the LaPaz basalts. Our lava flow model (Fig. 6) provides ample scope for such a cumulate-rich base. Additionally, NWA 3160 (a basaltic clast of NWA 2727), which has chemical affinities to NWA 773 (Zeigler et al. 2006), may represent another chilled portion of a putative lava flow, similar to NWA 032. NWA 3160 possesses dentritic olivines and pyroxenes in its groundmass that appear similar to olivines formed at cooling rates in excess of 60 °C $hr^{-1}$ in experimental charges (Lofgren et al. 1974; Donaldson et al. 1975). NWA 3160 also has euhedral phenocryst olivine grains with similar core compositions (~$Fo_{55-70}$) (Zeigler et al. 2006) to those seen in NWA 032. The lack of plagioclase and large pyroxenes in this sample may indicate that this represents the lowermost chill portion of an idealized model mare basalt flow, whereas NWA 032 represents the upper chill portion (Fig. 6).

The lunar lava flow model may provide a robust general representation from which to elucidate the relative relationships of lunar meteorites within their respective lava flows, even when they do not necessarily originate from the same flow on the Moon. Results for the LaPaz basalts and NWA 032 point to a lunar lava flow possessing a gross stratigraphy of a cumulate base and chilled margins, much like some large, thick terrestrial lava flows (e.g., Kirkpatrick 1977; Lentz et al. 1999). From the varied chemical composition of Apollo 12 and 15 low-Ti mare basalts, it has been inferred that shallow-level fractionation of olivine, pigeonite, and chromite occurred during their petrogenesis (e.g., Rhodes and Hubbard 1973; Rhodes et al. 1977). We suggest that our model for the stratigraphy of a lunar lava flow, based on low-Ti lunar mare basalt meteorites, may also apply to these rocks.

Many questions remain relating to physical processes involved with lunar mare basalt petrogenesis, including whether similar lava flow models might apply to high-Ti mare basalts, the causes of melting over prolonged periods (from ~4.5 to ~3.0 Gyr), the structural controls on volcanism, rates and scales of flow emplacement, and the effect and range of cooling rates on an airless body such as the Moon. Head and Wilson (1992) suggested that some lunar lava flows

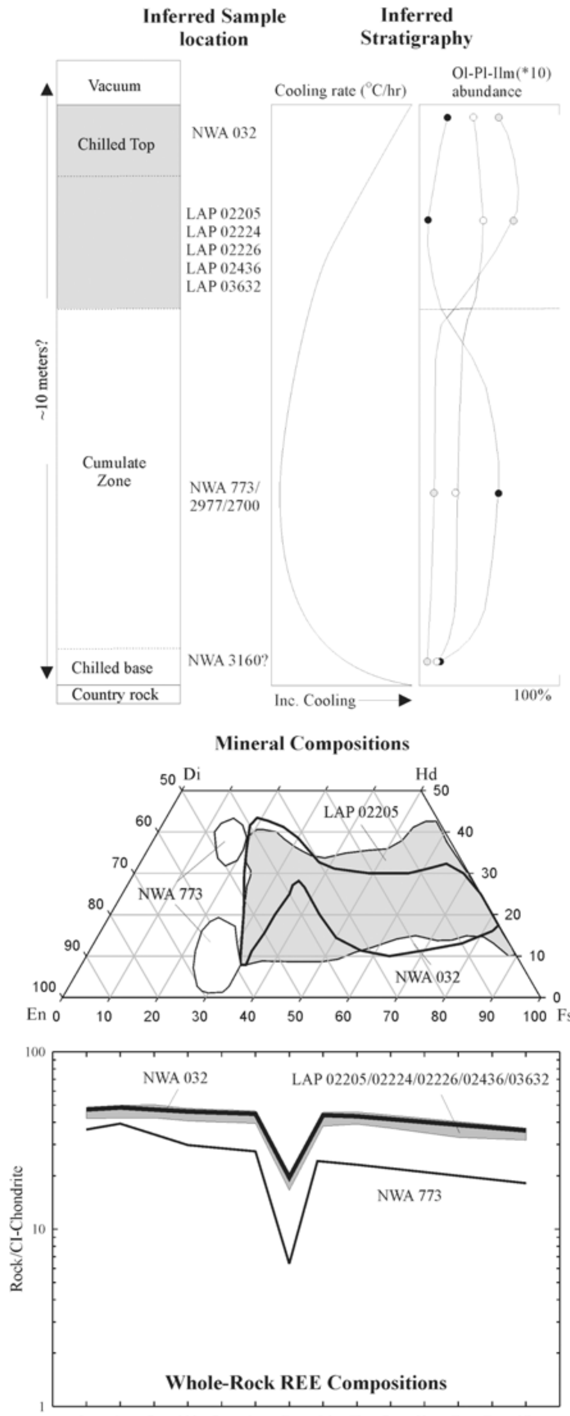


Fig. 6. A schematic model for the origin of an incompatible-element-enriched mare basalt lava flow ~3 Gyr on the Moon. Shown are the inferred positions of NWA 032, the LaPaz basalts, and other meteorites considered to be paired in the literature (see text for details). Although these meteorites may not be directly related, we suggest this model may apply as a gross structure for lava flows on the Moon. We summarize apparent variations in the putative mare lava flow subsequent to crystallization of olivine, pigeonite, and chromite at shallow levels in the lunar crust. Inferred stratigraphy illustrates variation in cooling rate within the flow, and modal mineralogy as a function of depth within the flow. Mineral compositions are most variable for pyroxene where they relate to the degree of accumulation (pigeonite and augite in NWA 773) and cooling rate (low CaO ferropyroxenes in NWA 032). Rare earth element patterns are similar for NWA 032, LAP 02205/02224/02226/02436, and LAP 03632, and may relate to NWA 773 by crystal accumulation (and mineral dilution). Succeeding these events was the impact-induced shock of the basalts and the eventual expulsion of material into space prior to fall to Earth. Pyroxene compositions and whole-rock REE data are from Day et al. (2006b), and Fagan et al. (2002; 2003). The flow thickness estimate is based on cooling rate–flow thickness relations of Grove and Walker (1977), and the thickness of mare basalt flows imaged from Hadley Rille (Howard et al. 1972).

are similar in scale and dimension to some of the largest continental flood basalt lava flows on Earth (e.g., the Columbia River Roza flow) (Self et al. 1997), despite the low average flux rate estimated for the lunar mare (~$10^{-2}$ $km^3$/yr). Further studies of textures in lunar rocks are likely to provide new insight into the stratigraphy and petrogenesis of lunar mare basalts yielding constraints on the volcanic history of the Moon.

## CONCLUSIONS

Quantitative textural analysis of NWA 032 and the LaPaz basalts, in conjunction with whole-rock and mineral chemistry, provides persuasive evidence for their crater-source or launch pairing. Crystal size distribution measurements of NWA 032 imply a mixed population of slowly cooled phenocrysts and fast cooled matrix, whereas the population of crystals present in the LaPaz basalts indicates a single phase of nucleation and growth. Spatial distribution patterns for the meteorites, when considered together, indicate the clumping and formation of clustered crystal frameworks in their respective melts succeeded by continued nucleation and growth of crystals. This process has resulted in increasingly poor sorting and clumping during competition for growth with crystallization of the melt. We provide a new model to explain the different crystal populations for NWA 032 and the LaPaz basalts, which involves the crystallization of early formed phenocrysts at hypabyssal depths in the lunar crust followed by eruption and flow differentiation on the surface (or in shallow level dykes and sills). We suggest that differentiation of the flow would allow a cumulate base and variable cooling, explaining the textures and modal mineralogies of mare basalts. Potentially, this model allows a framework for linking mare basalt meteorites (as well as Apollo low-Ti basalts), resulting in better understanding of volcanic processes on the Moon.

*Acknowledgments*–We are grateful to J. Clark, D. Chertkoff, E. Hill, D. Jerram, A. Mock, and D. Morgan for assistance, comments, and discussions relating to quantitative textural analysis. Editorial handling by R. Korotev and the reviews and suggestions of J. Boesenberg, K. Righter, G. Lofgren, and T. Jull improved the quality of this work. This research has been supported by NASA Cosmochemistry grant NNG 5GG-03G to L. Tyler.

*Editorial Handling*—Dr. Randy Korotev

## REFERENCES

Anand M., Taylor L. A., Floss C., Neal C. R., Terada K., and Tanikawa S. 2006. Petrology and geochemistry of LaPaz Icefield 02205: A new unique low-Ti mare-basalt meteorite. *Geochimica et Cosmochimica Acta* 70:246–264.

Borg L. E., Shearer C. K., Asmerom Y., and Papike J. J. 2004. Prolonged KREEP magmatism on the Moon indicated by the youngest dated lunar igneous rock. *Nature* 432:209–211.

Bunch T. E., Wittke J. H., Korotev R. L., and Irving A. J. 2006. Lunar meteorites NWA 2700, NWA 2727, and NWA 2977: Mare basalt/gabbro breccias with affinities to NWA 773 (abstract #1375). 37th Lunar and Planetary Science Conference. CD-ROM.

Cashman K. V. 1993. Relationship between plagioclase crystallization and cooling rate in basaltic melts. *Contributions to Mineralogy and Petrology* 113:126–142.

Cashman K. V. and Marsh B. D. 1988. Crystal size distribution (CSD) in rocks and the kinetics and dynamics of crystallization. *Contributions to Mineralogy and Petrology* 99:292–305.

Cushing J. A., Taylor G. J., Norman M. D., and Keil K. 1999. The granulitic impactite suite: Impact melts and metamorphic breccias of the early lunar crust. *Meteoritics & Planetary Science* 34:185–195.

Day J. M. D., Taylor L. A., Hill E., and Liu Y. 2005. Textural analysis and crystallization histories of the La Paz mare basalt meteorites (abstract). *Meteoritics & Planetary Science* 40:A37.

Day J. M. D., Taylor L. A., Floss C., and McSween H. Y., Jr. 2006a. Petrology and chemistry of MIL 03346 and its significance in understanding the petrogenesis of nakhlites on Mars. *Meteoritics & Planetary Science* 41:581–606.

Day J. M. D., Taylor L. A., Floss C., Patchen A. D., Schnare D. W., and Pearson D. G. 2006b. Comparative petrology, geochemistry, and petrogenesis of evolved, low-Ti lunar mare basalt meteorites from the LaPaz icefield, Antarctica. *Geochimica et Cosmochimica Acta* 70:1581–1600.

Day J. M. D., Floss C., Taylor L. A., Anand M., and Patchen A. D. 2006c. Evolved mare basalt magmatism, high-Mg/Fe feldspathic crust, chondritic impactors, and the petrogenesis of Antarctic lunar meteorites Meteorite Hills 01210 and Pecora Escarpment 02007. *Geochimica et Cosmochimica Acta*, doi:10.1016/j.gca.2006.05.001.

Donaldson C. H. 1976. An experimental investigation of olivine morphology. *Contributions to Mineralogy and Petrology* 57: 187–213.

Donaldson C. H. 1979. An experimental investigation of the delay in nucleation of olivine in mafic magmas. *Contributions to Mineralogy and Petrology* 69:21–32.

Donaldson C. H., Usselman T. M., Williams R. J., and Lofgren G. E. 1975. Experimental modelling of the cooling history of Apollo 12 olivine basalts. Proceedings, 6th Lunar Science Conference. pp. 843–869.

Fagan T. J., Taylor G. J., Keil K., Bunch T. E., Wittke J. H., Korotev R. L., Jolliff B. L., Gillis J. J., Haskin L. A., Jarosewich E., Clayton R. N., Mayeda T. K., Fernandes V. A., Burgess R., Turner G., Eugster O., and Lorenzetti S. 2002. Northwest Africa 032: Product of lunar volcanism. *Meteoritics & Planetary Science* 37:371–394.

Fagan T. J., Taylor G. J., Keil K., Hicks T. L., Killgore M., Bunch T. E., Wittke J. H., Mittlefehldt D. W., Clayton R. N., Mayeda T. K., Eugster O., Lorenzetti S., and Norman M. D. 2003. Northwest Africa 773: Lunar origin and iron-enrichment trend. *Meteoritics & Planetary Science* 38:529–554.

Fernandes V. A. and Burgess R. 2006. Ar-Ar studies of two lunar mare rocks: LAP 02205 and EET 96008 (abstract #1145). 37th Lunar and Planetary Science Conference. CD-ROM.

Fernandes V. A., Burgess R., and Turner G. 2003. $^{40}Ar$-$^{39}Ar$ chronology of lunar meteorites Northwest Africa 032 and 773. *Meteoritics & Planetary Science* 38:555–564.

Grove T. L. and Walker D. 1977. Cooling histories of Apollo 15 quartz-normative basalts. Proceedings, 8th Lunar Science Conference. pp. 1501–1520.

Head J. W. III and Wilson L. 1992. Lunar mare volcanism:

Stratigraphy, eruption conditions and the evolution of secondary crusts. *Geochimica et Cosmochimica Acta* 56:2155–2175.

Higgins M. D. 2000. Measurement of crystal size distributions. *American Mineralogist* 85:1105–1116.

Higgins M. D. 2002. Closure in crystal size distributions (CSD), verification of CSD calculations, and the significance of CSD fans. *American Mineralogist* 87:171–175.

Howard K. A., Head J. W., and Swann G. A. 1972. Geology of Hadley Rille. Proceedings, 3rd Lunar Science Conference. pp. 1–14.

Jerram D. A., Cheadle M. J., Hunter R. H., and Elliott M. T. 1996. The spatial distribution of grains and crystals in rocks. *Contributions to Mineralogy and Petrology* 125:60–74.

Jerram D. A., Cheadle M. J., and Philpotts A. J. 2003. Quantifying the building blocks of igneous rocks: Are clustered crystal frameworks the foundation? *Journal of Petrology* 44:2033–2051.

Jolliff B. L., Korotev R. L., Zeigler R. A., and Floss C. 2003. Northwest Africa 773: Lunar mare breccia with a shallow-formed olivine-cumulate component, inferred very-low-Ti (VLT) heritage and a KREEP connection. *Geochimica et Cosmochimica Acta* 67:4857–4879.

Joy K. H., Crawford I. A., Downes H., Russell S. S., and Kearsley A. T. 2006. A petrological, mineralogical, and chemical analysis of the lunar mare basalt meteorite LaPaz Icefield 02205, 02224, and 02226. *Meteoritics & Planetary Science* 41:1003–1025.

Kirkpatrick R. J. 1977. Nucleation and growth of plagioclase, Makaopuhi and Alae lava lakes, Kilauea Volcano, Hawaii. *Geological Society of America Bulletin* 88:78–84.

Kirkpatrick R. J. 1981. Kinetics of crystallization of igneous rocks. In *Kinetics of geochemical processes,* edited by Lasaga A. and Kirkpatrick R. J. Washington, D.C.: Mineralogical Society of America. pp. 321–398.

Kirkpatrick R. J. 1983. Theory of nucleation in silicate melts. *American Mineralogist* 68:66–77.

Lentz R. C. F. and Taylor G. J. 2002. Petrographic textures and insights into basaltic lava flow emplacement on Earth, the Moon, and Vesta (abstract #1332). 33rd Lunar and Planetary Science Conference. CD-ROM.

Lentz R. C. F., Taylor G. J., and Treiman A. H. 1999. Formation of a Martian pyroxenite: A comparative study of the nakhlite meteorites and Theo's flow. *Meteoritics & Planetary Science* 34:919–932.

Lofgren G. E. 1980. Experimental studies on the dynamic crystallization of silicate melts. In *The physics of magmatic processes,* edited by Hargreaves R. B. Princeton, New Jersey: Princeton University Press. pp. 487–551.

Lofgren G., Donaldson C. H., Williams R. J., Mullins O., Jr., and Usselman T. M. 1974. Experimentally reproduced textures and mineral chemistry of Apollo 15 quartz normative basalts. Proceedings, 5th Lunar Science Conference. pp. 549–567.

Marsh B. D. 1988. Crystal size distribution (CSD) in rocks and the kinetics and dynamics of crystallization. *Contributions to Mineralogy and Petrology* 99:277–291.

Marsh B. D. 1998. On the interpretation of crystal size distributions in magmatic systems. *Journal of Petrology* 39:553–599.

Morgan D. and Jerram D. A. 2006. On estimating crystal shape for crystal size distribution analysis. *Journal of Volcanology and Geothermal Research* 154:1–7.

Nabelek P. I., Taylor L. A., and Lofgren G. E. 1978. Nucleation and growth of plagioclase and the development of textures in high-alumina basaltic melt. Proceedings, 9th Lunar and Planetary Science Conference. pp. 725–741.

Nishiizumi K. and Caffee M. W. 2001. Exposure histories of lunar meteorites Northwest Africa 032 and Dhofar 081 (abstract #2101). 32nd Lunar and Planetary Science Conference. CD-ROM.

Nishiizumi K., Hillegonds D. J., and Welten K. C. 2006. Exposure and terrestrial histories of lunar meteorites LAP 02205/02224/02226/02436, MET 01210, and PCA 02007 (abstract #2369). 37th Lunar and Planetary Science Conference. CD-ROM.

Nyquist L. E., Shih C.-Y., Reese Y., and Bogard D. D. 2005. Age of lunar meteorite LAP 02205 and implications for impact-sampling of planetary surfaces (abstract #1374). 36th Lunar and Planetary Science Conference. CD-ROM.

Onorato P. I. K., Uhlmann D. R., Taylor L. A., Coish R. A., and Gamble R. P. 1978. Olivine cooling speedometers. Proceedings, 9th Lunar and Planetary Science Conference. pp. 613–628.

Rankenburg K., Brandon A., Norman M., and Righter K. 2005. LAP 02205: An evolved member of the Apollo 12 olivine basalt suite? (abstract). *Meteoritics & Planetary Science* 40:A125.

Rhodes J. M. and Hubbard N. J. 1973. Chemistry, classification and petrogenesis of Apollo 15 mare basalts. Proceedings, 4th Lunar Science Conference. pp. 1127–1148.

Rhodes J. M., Blanchard D. P., Dungan M. A., Brannon J. C., and Rodgers K. V. 1977. Chemistry of Apollo 12 mare basalts: Magma types and fractionation processes. Proceedings, 8th Lunar Science Conference. pp. 1305–1338.

Righter K., Collins S. J., and Brandon A. D. 2005. Mineralogy and petrology of the LaPaz Icefield lunar mare basaltic meteorites. *Meteoritics & Planetary Science* 40:1703–1722.

Self S., Thordarson T., and Keszthelyi L. 1997. Emplacement of continental flood basalt lava flows. In *Large igneous provinces: Continental, oceanic and planetary flood volcanism.* Geophysical Monograph #100. Washington, D.C.: American Geophysical Union. pp. 381–410.

Taylor L. A., Patchen A., Taylor D. H. S., Chambers J. G., and McKay D. S. 1996. X-ray digital imaging petrography of lunar mare soils: Modal analysis of minerals and glasses. *Icarus* 124:500–512.

Usselman T. M., Lofgren G. E., Donaldson C. H., and Williams R. J. 1975. Experimentally reproduced textures and mineral chemistries of high-titanium mare basalts. Proceedings, 6th Lunar Science Conference. pp. 997–1020.

Zeigler R. A., Korotev R. L., Jolliff B. L., and Haskin L. A. 2005. Petrography and geochemistry of the LaPaz Icefield basaltic lunar meteorite and source-crater pairing with Northwest Africa 032. *Meteoritics & Planetary Science* 40:1073–1102.

Zeigler R. A., Korotev R. L., Irving A. J., Jolliff B. L., Kuehner S. M., and Hupé A. C. 2006. Petrography and composition of lunar basaltic meteorite NWA 3160 (abstract #1804). 37th Lunar and Planetary Science Conference. CD-ROM.